Protective Effects and Mechanism of Hydroxylpurpurin on H_2O_2-Induced Oxidative Stress Injury in Skin

Meigui YOU
Fujian Province University
Jiaqi He
Fujian Province University
Weiqing LUO
Fujian Province University
Liangyingjun LUO
Fujian Province University
Jinhui LI
Fujian Province University
Jiajia LI
Fujian Province University
Yaping XU
ypxu@xmmc.edu.cn
Fujian Province University

Article

Keywords: Hydroxylpurpurin, Skin oxidative stress, Endocannabinoid system, PI3K/AKT signaling pathway, Network pharmacology

Posted Date: March 6th, 2026

DOI: https://doi.org/10.21203/rs.3.rs-8798539/v1

Additional Declarations: No competing interests reported.

Version of Record: A version of this preprint was published at Scientific Reports on August 14th, 2026. See the published version at https://doi.org/10.1038/s41598-026-66369-5.

Protective Effects and Mechanism of Hydroxylpurpurin on H_2O_2-Induced Oxidative Stress Injury in Skin

Meigui YOU[1,2‡], Jiaqi He[1,2],Weiqing LUO[1,2], Liangyingjun LUO[1,2], Jinhui LI[1,2], Jiajia LI [1,2], Yaping XU[1,2,*]

1 Key Laboratory of Functional and Clinical Translational Medicine, Fujian Province University, Xiamen Medical College, Xiamen 361023, China

2 Institute of Respiratory Diseases Xiamen Medical College, Xiamen 361023; China

* For correspondence: Meigui YOU, ymg0501@163.com;
Yaping XU,ypxu@xmmc.edu.cn

Abstract

The skin serves as the primary barrier protecting the body from environmental insults and is highly susceptible to oxidative stress induced by excessive production of reactive oxygen species (ROS), which contributes to skin aging and inflammatory skin disorders. The endocannabinoid system (ECS) plays a critical role in regulating skin inflammation and oxidative stress; however, natural compounds targeting this system remain largely unexplored. Hydroxylpurpurin, a natural anthraquinone compound isolated from Rubia cordifolia L., exhibits potent antioxidant activity, but its protective mechanism against skin oxidative stress has not been fully elucidated.In this study, an integrated strategy combining network pharmacology, molecular docking, and experimental validation was employed to investigate the molecular mechanisms underlying the antioxidant effects of hydroxylpurpurin. Network pharmacology analysis and Molecular docking revealed that the potential targets of hydroxylpurpurin associated with skin oxidative stress were significantly enriched in the PI3K/AKT signaling pathway, suggesting its pivotal involvement in the protective effects of hydroxylpurpurin. Moreover, experimental validation using an oxidative stress model in HaCaT keratinocytes showed that hydroxylpurpurin markedly reduced intracellular ROS levels and alleviated oxidative stress-induced cellular damage. Collectively, these findings indicate that hydroxylpurpurin may exert its antioxidant effects by modulating ECS-related targets and activating the PI3K/AKT signaling pathway, providing novel insights into its potential application for the prevention and treatment of skin oxidative stress-related disorders.

Key Words: Hydroxylpurpurin; Skin oxidative stress; Endocannabinoid system; PI3K/AKT signaling pathway; Network pharmacology

1.Introduction

The skin, as the largest organ of the human body, constitutes the first barrier between the body and the external environment and is therefore highly susceptible to both endogenous and exogenous stimuli, which may lead to excessive accumulation of reactive oxygen species (ROS) and subsequent oxidative stress[1]. Oxidative stress refers to a pathological state in which excessive production of intracellular ROS or depletion of antioxidant defenses disrupts the cellular redox balance. Under such conditions, ROS induce damage to lipids, DNA, and proteins, thereby impairing cellular homeostasis and triggering a series of stress responses[2]. Excessive ROS generation can result in cellular senescence, injury, and death, ultimately contributing to the development of various skin disorders, including skin aging, inflammatory skin diseases, and epidermal tumors[3].

The endocannabinoid system (ECS) is one of the key regulatory systems involved in skin inflammation and immune responses[4]. It mainly consists of endogenous cannabinoids, including N-arachidonoylethanolamide (anandamide, AEA) and 2-arachidonoylglycerol (2-AG), cannabinoid receptors CB1 and CB2, as well as the enzymes responsible for their synthesis and degradation[5, 6]. Accumulating evidence indicates that activation of ECS receptors can protect serum-deprived astrocytes from H_2O_2-induced apoptosis[7]. Moreover, the ECS ligands AEA and 2-AG can modulate the activity of several antioxidant enzymes by targeting cannabinoid receptors CB1 and CB2, as well as other related receptors, thereby reducing ROS levels and exerting cytoprotective effects[8].

China possesses abundant traditional Chinese medicinal (TCM) resources, whose efficacy and safety have been extensively documented. Given the limitations of synthetic antioxidants, such as high cost and potential toxic side effects, increasing attention has been directed toward natural antioxidants derived from traditional medicinal plants[9]. Current studies have primarily focused on active components such as flavonoids, phenolic acids, saponins, polysaccharides, vitamins and trace elements, and terpenoids. These compounds exert protective effects mainly by scavenging free radicals; however, their antioxidant mechanisms are not identical. Therefore, from the perspective of ECS-mediated regulation of skin oxidative stress injury, the present study screened 440 plant-derived monomeric compounds to identify candidates with significant protective effects, aiming to provide experimental evidence for the clinical treatment of skin oxidative stress injury and to support further drug development.

Rubia cordifolia L., a perennial herb belonging to the Rubiaceae family, is a commonly used traditional Chinese medicinal plant. Its roots and rhizomes possess pharmacological properties such as cooling the blood, removing blood stasis, stopping bleeding, and promoting circulation[10]. Pharmacological studies have demonstrated that Rubia cordifolia exhibits antibacterial, antiviral, anti-inflammatory, antitumor, antioxidant, and immunomodulatory activities[11-15]. Hydroxylated alizarin (Hydroxylpurpurin) is a natural anthraquinone isolated from the roots of Rubia cordifolia[16]. The 2015 edition of the Chinese Pharmacopoeia lists hydroxylated alizarin and purpurin as the main quality control markers of Rubia cordifolia[17]. Both compounds

possess antioxidant and enzyme-inhibitory activities, with hydroxylated alizarin exhibiting stronger inhibitory effects[18]. In addition, emodin, another anthraquinone compound widely studied in modern pharmacology, has been shown to exert anti-inflammatory and antioxidant effects by reducing ROS production during inflammatory processes[19].

Currently, research on hydroxylated alizarin has mainly focused on its extraction[20], while studies on its antioxidant application remain limited. Moreover, its precise molecular targets and potential signaling pathways involved in antioxidant activity have not yet been fully elucidated. Therefore, in this study, network pharmacology was first employed to identify potential targets of hydroxylated alizarin in the treatment of skin oxidative stress injury, followed by molecular docking analysis to verify its binding affinity with core target proteins from a structural biology perspective. Subsequently, the protective effects and key signaling pathways were experimentally validated using an H_2O_2-induced oxidative stress model in HaCaT cells, with further investigation into the involvement of the endocannabinoid system (ECS). Through an integrated strategy combining "network prediction–molecular simulation–experimental validation," this study aims to provide multidimensional theoretical support and experimental evidence for elucidating the antioxidant mechanisms of hydroxylated alizarin.

2. Materials and methods

2.1 Drugs and Reagents

Hydroxylpurpurin was purchased from Cayman Chemical (batch no. 35033) with a purity of ≥98%. Hydroxylpurpurin appearing as a brown crystalline powder, and was dissolved in dimethyl sulfoxide (DMSO) to prepare a 200 mmol/L stock solution, which was stored at −20 °C. High-glucose DMEM was obtained from Dalian Meilun Biotechnology Co., Ltd.; fetal bovine serum was purchased from Jiangsu Enmo Assay Biotechnology Co., Ltd.; trypsin and CCK-8 were purchased from Dalian Meilun Biotechnology Co., Ltd. The Annexin V-FITC/PI apoptosis detection kit was obtained from Roche (Switzerland); the reactive oxygen species (ROS) detection kit was purchased from Solarbio (China); the cDNA reverse transcription kit was obtained from TaKaRa; the universal fluorescent quantitative PCR kit was purchased from Biosharp (China); GAPDH primers were obtained from Tsingke Biotechnology; primers for FAAH, NAAA, NAPE-PLD, CB1/CB2, and ASAH were obtained from GeneCreate Biotech; 4% paraformaldehyde solution was purchased from Solarbio. All other reagents were of analytical grade and commercially available.

2.2 Instruments

Class II biological safety cabinet (Shanghai Zhicheng Analytical Instrument Manufacturing Co., Ltd.), CO_2 incubator (Thermo Fisher Scientific), research-grade inverted microscope (Carl Zeiss AG, Germany), fluorescence microscope (Leica), multifunctional microplate reader (Molecular Devices), automated cell counter (Guangzhou Boda Boju Technology Co., Ltd.), flow cytometer (Beckman Coulter),

nucleic acid concentration analyzer (Quawell, USA), gradient PCR thermal cycler (Bio-Rad, USA), and real-time fluorescence quantitative PCR system (Roche, Switzerland).

2.3 Identification of Compound Targets and Disease Targets

The SMILES structure of hydroxylated alizarin was uploaded to the SwissTarget Predictiondatabase (http://www.swisstargetprediction.ch/) for target prediction[21].

Using "skin aging" as the keyword, human genes associated with the disease were retrieved from the GeneCards database (https://www.genecards.org/)[22], OMIM (https://www.omim.org/)[23], and DrugBank (https://go.drugbank.com/)[24] to obtain disease-related targets.

2.4 Venn Diagram Analysis and PPI Network Construction

Venn diagrams of compound-related targets and disease-related targets were generated using Venny 2.1 software to identify the overlapping targets.

The common targets between the drug and the disease were imported into the STRING database (https://string-db.org/cgi/input.pl)[25] for protein–protein interaction (PPI) network construction. The organism was set to *Homo sapiens* to obtain the PPI network.

2.5 GO and KEGG Pathway Enrichment Analysis

Gene Ontology (GO) and Kyoto Encyclopedia of Genes and Genomes (KEGG) pathway enrichment analyses were performed using the Bioconductor bioinformatics package in R 4.4.0. A significance threshold of $P < 0.05$ was applied.

2.6 Molecular Docking

The crystal structures of AKT1(PDB ID 4GV1[26]) and PIK3CA(PDB ID 7JIU[27]) used for molecular docking were obtained from the Protein Data Bank (PDB). The three-dimensional structure of the small molecule purpurin was downloaded from the PubChem database and subjected to energy minimization under the MMFF94 force field[28].

Molecular docking was performed using AutoDock Vina 1.2.7[29]. Prior to docking, the receptor proteins were prepared using PyMOL 2.5.2[30], including removal of water molecules, salt ions, and co-crystallized ligands. The docking grid box was then set to encompass the crystal ligand. Subsequently, ADFRsuite version 1.0[31] was used to convert all processed ligands and receptor proteins into the PDBQT format required for AutoDock Vina 1.2.7. During docking, the exhaustiveness parameter was set to 32, while all other parameters were kept at their default values. The docking conformation with the highest binding score was considered the optimal binding pose, and the final docking results were visualized and analyzed using PyMOL 2.5.2.

2.7 Cell Culture

HaCaT cells were kindly provided by the Third Institute of Oceanography, Ministry of Natural Resources. HaCaT cells were cultured in RPMI-1640 or DMEM medium supplemented with 10% fetal bovine serum and 1% penicillin–streptomycin in a humidified incubator at 37 °C with 5% CO_2. As adherent cells, HaCaT cells were passaged and the culture medium was refreshed every 2–3 days.

2.8 CCK-8 Assay for Cell Viability after H_2O_2 Treatment at Different Concentrations

HaCaT cells were seeded into 96-well plates at a density of 1×10^4 cells per well and cultured for 24 h. H_2O_2 solutions at concentrations of 0 μM, 100 μM, 200 μM, 400 μM, 600 μM, and 800 μM were prepared in complete DMEM medium and added to the cells by medium replacement, with a final volume of 100 μL per well. The cells were then incubated at 37 °C in a humidified atmosphere containing 5% CO_2 for 24 h.

Subsequently, a 10% CCK-8 working solution was prepared using basal DMEM medium. The culture medium was removed, the cells were washed once with 1× PBS, and then incubated with the CCK-8 working solution at 37 °C for 1 h in the dark. The absorbance was measured at 450 nm using a microplate reader, and cell viability was calculated accordingly.

2.9 Flow Cytometric Analysis of Intracellular ROS Levels Induced by Different Concentrations of H_2O_2

When cells reached 80–90% confluence, they were trypsinized, collected, and resuspended in 1 mL of complete medium. Complete medium (2 mL per well) was added in advance to 6-well plates, and 90 μL of the cell suspension was added to each well with gentle shaking to ensure uniform distribution. The remaining cells were used for passaging. Cell density and distribution were observed under a microscope, and the cells were incubated at 37 °C with 5% CO_2 for 24 h.

H_2O_2 solutions at concentrations of 0 μM, 100 μM, 200 μM, 400 μM, 600 μM, and 800 μM were prepared in complete DMEM medium and added by medium replacement. After 24 h of treatment, cells were collected by centrifugation at 4 °C and 400 g for 3 min. A blank group (without probe loading) and experimental groups were set up, with the blank group used for voltage adjustment. Cells were washed once with pre-cooled PBS and centrifuged under the same conditions. After removing PBS, the DCFH probe was diluted 1:1000 in basal DMEM medium and added to the cells (500 μL per well). Cells were incubated at 37 °C in the dark for 30 min, with gentle inversion every 5 min to ensure sufficient contact between cells and the probe. Cells were then centrifuged at 400 g for 3 min, washed twice with 1× PBS, resuspended in 300 μL PBS, and analyzed by flow cytometry. Data were processed using FlowJo version 10.8.1.

2.10 Flow Cytometric Analysis of Apoptosis and ROS Levels under Hydroxylpurpurin Intervention

When cells reached 80–90% confluence, they were trypsinized, collected, and resuspended in 1 mL of complete medium. Complete medium (2 mL per well) was added in advance to 6-well plates, and 90 μL of the cell suspension was added to each well with gentle shaking. The remaining cells were used for passaging. After observing cell density and distribution under a microscope, cells were incubated at 37 °C with 5% CO_2 for 24 h. Cells were then collected by centrifugation at 400 g for 3 min and divided equally into two portions per well for ROS and apoptosis analyses.

The following groups were established: blank group (for voltage adjustment), control group, 600 μM H_2O_2 treatment group, 10 μM Hydroxylpurpurin treatment group, and 10 μM Hydroxylpurpurin + 600 μM H_2O_2 treatment group. Cells were washed once

with pre-cooled PBS and centrifuged under the same conditions. After removing PBS, the DCFH probe was diluted 1:1000 in basal DMEM medium and added to the cells (500 μL per well). For apoptosis detection, Annexin V dye, PI dye, and incubation buffer were mixed at a ratio of 10 μL:10 μL:1 mL, and 400 μL of the staining solution was added per well. Cells were incubated at 37 °C in the dark for 30 min, with gentle inversion every 5 min. Subsequently, cells were centrifuged at 4 °C and 400 g for 3 min, washed twice with PBS, resuspended in 300 μL PBS, and analyzed by flow cytometry. Data were processed using FlowJo version 10.8.1.

2.11 Fluorescence Imaging of Intracellular ROS after Hydroxylpurpurin Treatment

Cell seeding and drug treatments in 6-well plates were performed as described in Section 2.3. After 24 h of treatment, the culture medium was discarded, and cells were washed twice with pre-cooled PBS. The DCFH probe was diluted 1:1000 in pre-cooled PBS and added to each well (1.5 mL per well). Cells were incubated at 37 °C in the dark for 30 min, and fluorescence images were captured using a fluorescence inverted microscope.

2.12 LC–MS/MS Analysis of ECS-Related Lipid Levels after Hydroxylpurpurin Treatment

The following groups were established: control group, 600 μM H_2O_2 treatment group, 10 μM Hydroxylpurpurin treatment group, and 10 μM Hydroxylpurpurin + 600 μM H_2O_2 treatment group, with five parallel samples per group using 10 cm culture dishes. Cells were cultured, and logarithmic-phase cells were passaged at 30% confluence, yielding a total of 20 culture dishes. After 24 h, cells were pretreated with the effective plant monomer at a final concentration of 10 μM for 2 h, followed by stimulation with 600 μM H_2O_2 for 24 h. Cells were then observed, collected, and extracted using a methanol:water (1:1, v/v) solution. An internal standard was added at 0.5 μL per sample, followed by thorough mixing.

Each sample was extracted with 2 mL of solvent and subjected to ultrasonic disruption. An aliquot of 50 μL supernatant was used for protein quantification by the BCA method, and the remaining extract was mixed with 4 mL dichloromethane, centrifuged at 4 °C and 3000 rpm for 10 min, and the lower organic phase was collected. The solvent was evaporated under nitrogen, and each sample was reconstituted in 1 mL dichloromethane, passed through a column, evaporated again under nitrogen, and finally reconstituted in 200 μL of dichloromethane:methanol (9:1, v/v). Samples were sealed and stored before being sent for LC–MS/MS analysis.

2.13 RT-qPCR Analysis of ECS-Related Receptor and Enzyme Gene Expression after Hydroxylpurpurin Treatment

Total RNA was extracted from cells using an RNA extraction kit, and RNA concentration and purity were determined. Reverse transcription was performed to synthesize cDNA using a cDNA reverse transcription kit (TaKaRa) according to the manufacturer's instructions. Quantitative PCR reactions were prepared using a universal fluorescent qPCR kit (Biosharp, China), and mRNA expression levels of CB1, CB2, FAAH, NPLD, NAAA, and ASAH were measured using a real-time fluorescence

quantitative PCR system. Primers were synthesized by GeneCreate Biotech, and the primer sequences are listed in Table 1.

Table 1. The primer sequences.

Gene name	Primer sequence
CB_1 forward	5'-CCACTCCCGCAGCCTCCG-3'
CB_1 reverse	5'-ATCAGGCAAAACGCCACCAC-3'
CB_2 forward	5'-GGTGACAGAGATAGCCAATG-3'
CB_2 reverse	5'-GCCAATGAACAGGTATGAGG-3'
FAAH forward	5'-GAACTGCAGCACGAGATCGA-3'
FAAH reverse	5'-CCCTCCACTGGCAATCA-3'
NPLD forward	5'-AATCCGTGGCCAACATGGA-3'
NPLD reverse	5'-TTGGACCCATGTACCTGCGATG-3'
NAAA forward	5'-CAACCTGGCCTACGAGTCC-3'
NAAA reverse	5'-GCTTGCGTAAGACATTCCCAAAA-3'

2.14 Statistical Analysis

Statistical analysis was performed using GraphPad Prism 5.0. Data are presented as the mean ± SEM. Differences between groups were analyzed using the unpaired *t*-test and one-way analysis of variance (ANOVA). A P value < 0.05 was considered statistically significant.

3. Results and discussions

3.1 Identification of key targets

To comprehensively elucidate the chemical characteristics and pharmacological effects of hydroxylated alizarin, a total of 105 potential targets were predicted and screened using the SwissTargetPrediction database. In addition, 11,823 targets associated with oxidative stress–induced skin injury were retrieved from three databases (GeneCards, OMIM, and DrugBank). After further screening, 75 overlapping targets were ultimately identified as potential therapeutic targets for skin aging (Figure 1A).

As shown in the PPI network (Figure 1B), PIK3CA, PIK3CB, PIK3CD, PIK3R1, and PIK3R2 were located at the core of the network, suggesting that the PI3K complex may play a critical role in this process.

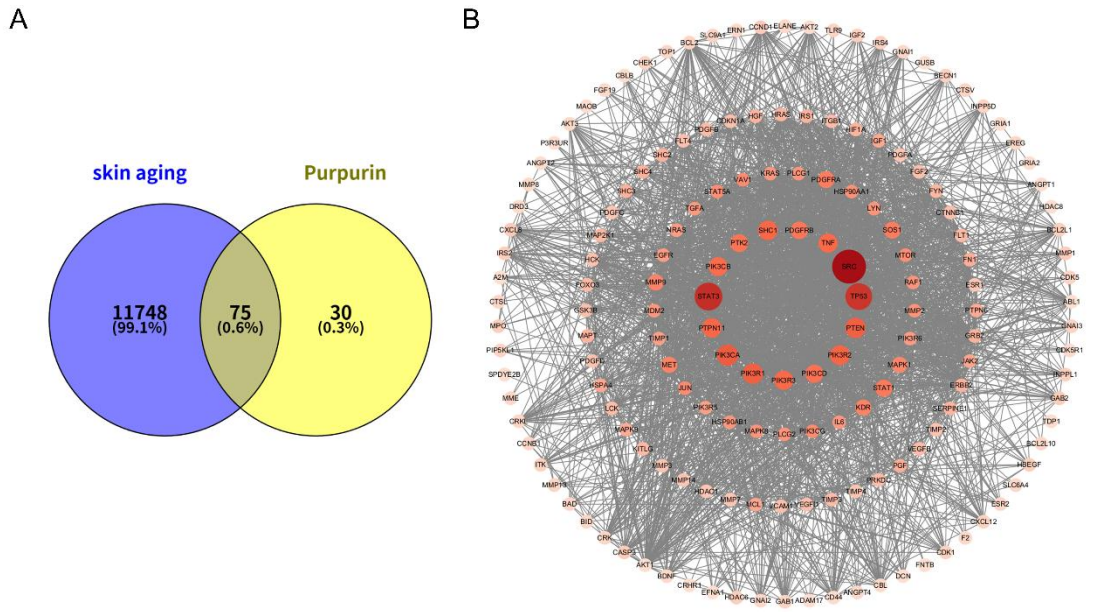

Figure 1. (A) Venn diagram; (B) protein–protein interaction (PPI) network.

3.2 GO and KEGG Pathway Analysis

As shown in Figure 2, Genomes (KEGG) enrichment and Gene Ontology (GO) and Kyoto Encyclopedia of Genes analyses were performed on the overlapping targets. The KEGG enrichment results (Figure 2A) indicated that the overlapping targets were significantly enriched in multiple signaling pathways related to skin injury, among which the PI3K–AKT signaling pathway ranked prominently, suggesting that this pathway may play an important role in the associated biological processes. The GO enrichment analysis (Figure 2B) revealed that the differentially expressed genes were mainly involved in key biological processes such as apoptosis and were closely associated with cellular signal transduction and regulatory functions.

Taken together, these findings suggest that the protective effects of hydroxylated alizarin against hydrogen peroxide–induced skin injury may be closely related to the regulation of the PI3K/AKT signaling pathway and apoptosis-related processes.

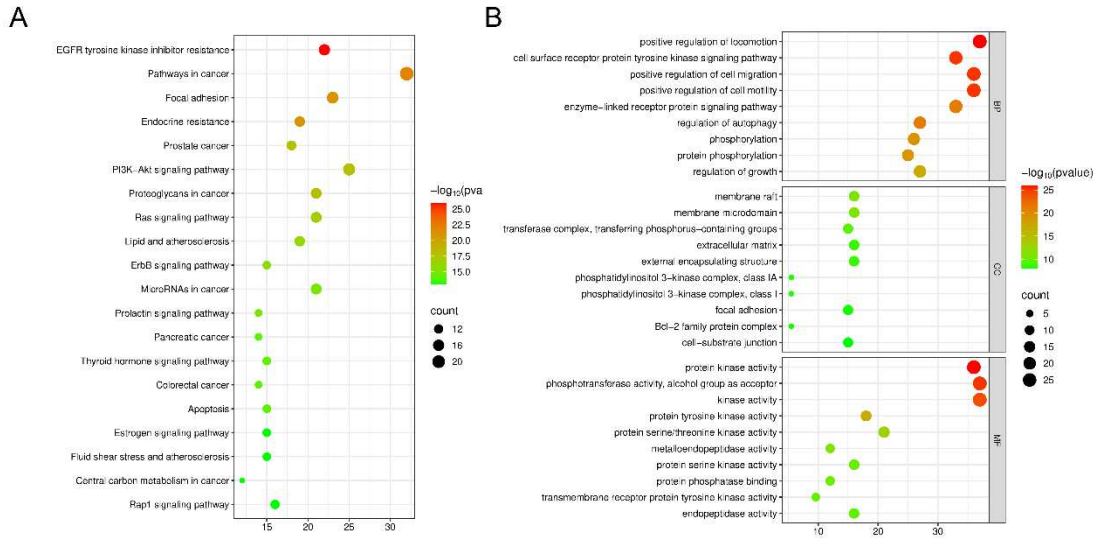

Figure 2. (A) KEGG pathway enrichment analysis of the overlapping targets; (B) GO enrichment analysis of the overlapping targets.

3.3 Analysis of the Binding of Hydroxylpurpurin and PI3K/AKT

Based on the above GO and KEGG enrichment analyses, which indicated that the PI3K/AKT signaling pathway plays an important role in the regulatory effects of hydroxylated alizarin on skin injury, representative core targets within this pathway, AKT1 and PIK3CA, were selected for molecular docking with purpurin to explore the potential molecular basis of their interactions.

As shown in Figure 3A, in the AKT1–purpurin complex, purpurin mainly binds to the AKT1 protein through hydrophobic interactions involving key residues such as ALA-177, THR-291, VAL-164, and THR-211. These hydrophobic residues collectively form a relatively stable hydrophobic binding pocket that facilitates ligand insertion and stabilization, thereby enhancing the binding stability between purpurin and AKT1. Although no obvious hydrogen bonds, π–π stacking interactions, or salt bridges were observed, hydrophobic interactions dominate the binding mode of this

complex, suggesting that purpurin may primarily rely on hydrophobic forces to achieve effective binding to AKT1.

As shown in Figure 3B, in the PIK3CA–purpurin complex, both hydrophobic interactions and hydrogen bonds were observed between purpurin and the PIK3CA protein. Specifically, residues ILE-848, ILE-932, TRP-780, and TYR-836 formed prominent hydrophobic interactions with the ligand, while VAL-851 and SER-854 interacted with purpurin via hydrogen bonds. The hydrophobic interactions provide a stable binding environment that promotes effective positioning of the ligand within the active pocket, while the hydrogen bonds further enhance binding directionality and overall stability. Overall, purpurin exhibits strong binding capability within the active pocket of PIK3CA, characterized by cooperative stabilization through hydrophobic interactions and hydrogen bonding.

The molecular docking results showed that the docking scores of purpurin with AKT1 and PIK3CA were −7.814 kcal/mol and −7.935 kcal/mol, respectively, indicating favorable binding affinities. Combined with the significant enrichment of the PI3K/AKT signaling pathway identified in the enrichment analyses, these findings further suggest that purpurin may stably interact with key proteins in the PI3K/AKT pathway. This provides molecular-level support for its potential involvement in skin injury and skin aging–related biological processes through modulation of the PI3K/AKT signaling axis. To further validate the biological relevance of the network pharmacology and molecular docking results, an oxidative stress model was subsequently established in HaCaT cells to experimentally verify the protective effects of hydroxylated alizarin.

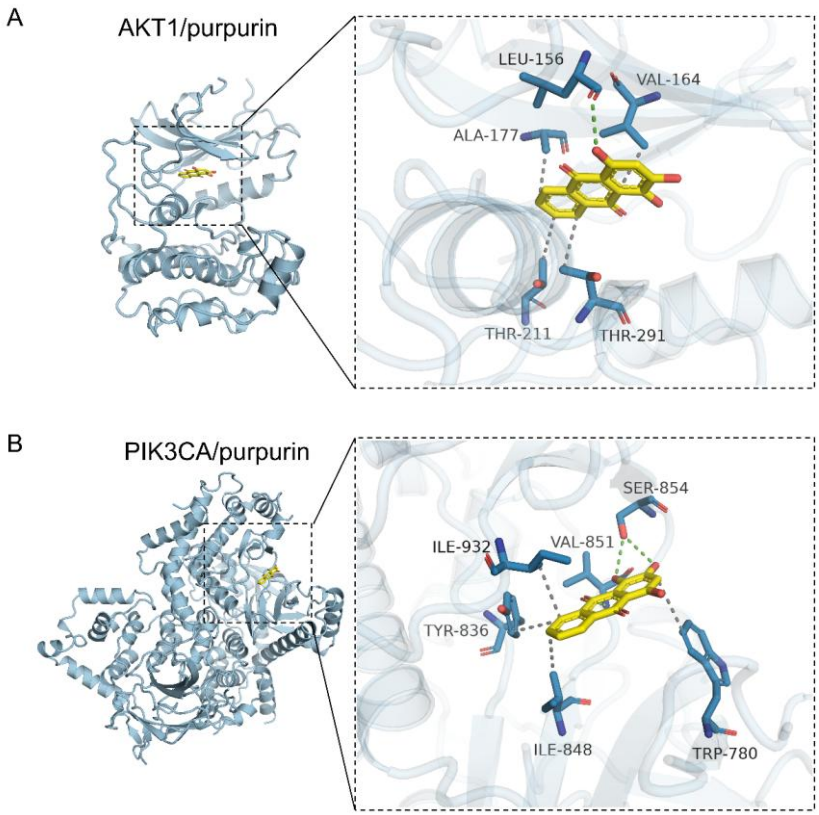

Figure 3. (A) Docking-derived binding mode of AKT1 with purpurin; (B) docking-derived binding mode of PIK3CA with purpurin. The yellow sticks represent the small molecule ligand, the light blue cartoon represents the protein, blue dashed lines indicate hydrogen bonds, and gray dashed lines indicate hydrophobic interactions.

3.4 Evaluation of the Oxidative Stress Model in HaCaT Cells

As shown in Figure 4A, compared with the control group, treatment with 100 μM and 200 μM H_2O_2 did not significantly affect the viability of HaCaT cells. In contrast, treatment with 400 μM, 600 μM, and 800 μM H_2O_2 resulted in a significant decrease in cell viability ($P < 0.001$) in a dose-dependent manner. When the concentration of H_2O_2 reached 600 μM, cell viability was reduced to approximately 50%. As shown in Figures 4B and 4C, intracellular ROS levels were not significantly altered by 100 μM or 200 μM H_2O_2 treatment, whereas exposure to 400 μM, 600 μM, and 800 μM H_2O_2 led to a marked increase in the mean fluorescence intensity of ROS ($P < 0.0001$), also in a dose-dependent manner.

Hydrogen peroxide is a commonly used exogenous agent for modeling skin oxidative stress. Previous studies have shown that approximately 1.5%–5% of oxygen consumption in the skin is converted into ROS, and excessive accumulation of ROS can trigger various skin disorders. In the present study, cell viability and ROS levels were used as evaluation indices, and the results confirmed that 600 μM H_2O_2 induced significant oxidative damage. Therefore, this concentration was selected to establish the oxidative stress model for subsequent experiments.

Hydroxylpurpurin Reduces H_2O_2-Induced Intracellular ROS Levels in HaCaT Cells.Figure 4D shows the changes in intracellular ROS levels observed under a fluorescence microscope. Compared with the 600 μM H_2O_2 treatment group, cells treated with 10 μM hydroxylated alizarin exhibited a markedly reduced ROS fluorescence intensity. Consistent results were obtained from flow cytometric analysis of ROS levels in HaCaT cells (Figure 4E), showing a significant decrease in intracellular ROS content following hydroxylated alizarin treatment. These findings indicate that hydroxylated alizarin effectively attenuates H_2O_2-induced oxidative stress in HaCaT cells.Among the 440 screened natural plant-derived monomeric compounds, hydroxylated alizarin emerged as a prominent candidate. Owing to its chemical stability and strong antioxidant activity, the present results provide direct evidence that hydroxylated alizarin can effectively inhibit ROS generation, thereby alleviating the degree of oxidative stress in HaCaT cells.

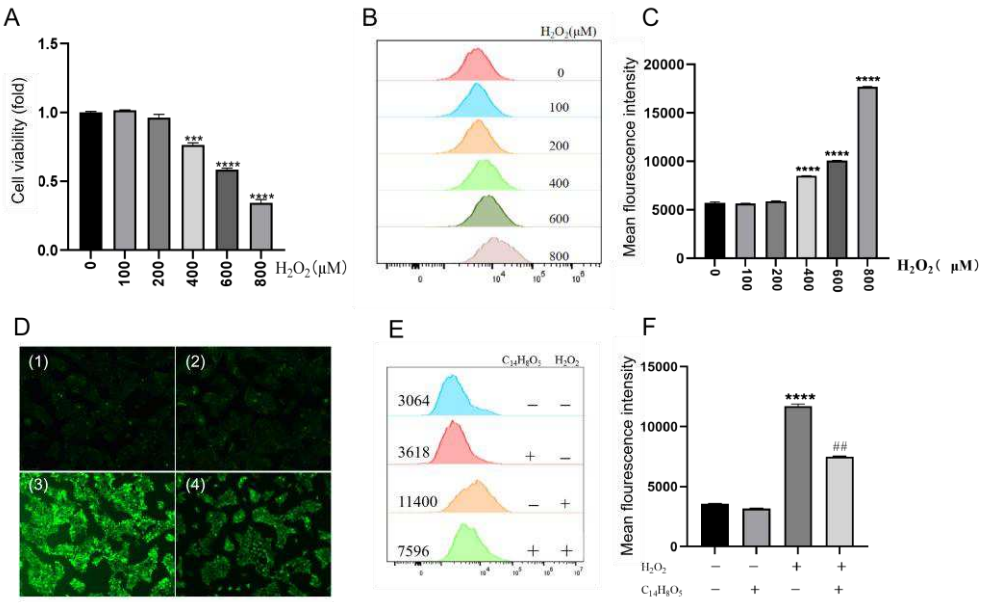

Figure 4. (A) Cell viability of HaCaT cells treated with different concentrations of hydrogen peroxide. (B) Flow cytometry fluorescence histogram; (C) statistical analysis ($\bar{x} \pm s$, n = 3), ***P < 0.001, ****P < 0.0001 vs. control group. (D) ROS distribution in HaCaT cells: (1) control group; (2) 10 μM Hydroxylpurpurin treatment group; (3) 600 μM H_2O_2 treatment group; (4) 10 μM Hydroxylpurpurin + 600 μM H_2O_2 treatment group; DCFH was used as the fluorescent probe. (E) Flow cytometric analysis of intracellular ROS in HaCaT cells. (F) Quantification of fluorescence intensity.****P < 0.0001 vs. control group; ##P < 0.01 vs. 600 μM H_2O_2 treatment group;

3.5 Hydroxylpurpurin Ameliorates H_2O_2-Induced Apoptosis in HaCaT Cell

As shown in Figure 5A, morphological changes of HaCaT cells before and after treatment were observed. Compared with the control group, treatment with 600 μM H_2O_2 resulted in a marked increase in cell death, characterized by reduced cellular translucency, progressive detachment, and cellular fragmentation. In contrast, compared with the 600 μM H_2O_2 model group, pretreatment with hydroxylated alizarin markedly reduced the number of dead cells, indicating an obvious protective effect against H_2O_2-induced cellular damage.

Figure 5B-C shows the apoptotic status of HaCaT cells following injury induced by 600 μM H_2O_2 with or without treatment with 10 μM Hydroxylpurpurin. As shown, compared with the control group, the apoptotic rate of HaCaT cells in the 600 μM H_2O_2 treatment group increased markedly from 2.29% to 21.08%. In contrast, the apoptotic rate in the 10 μM Hydroxylpurpurin pretreatment group was reduced to 9.58%, which was significantly lower than that in the H_2O_2 model group. These results indicate that hydroxylated alizarin can significantly attenuate H_2O_2-induced cellular injury by reducing the number of apoptotic cells, thereby exerting a protective effect. The experimental data, including the increase in cell viability (41%–66%) and the reduction of apoptosis to 9.58%, further confirm the protective efficacy of hydroxylated alizarin on skin-derived cells, suggesting that it rescues cells under oxidative damage primarily by suppressing apoptosis.

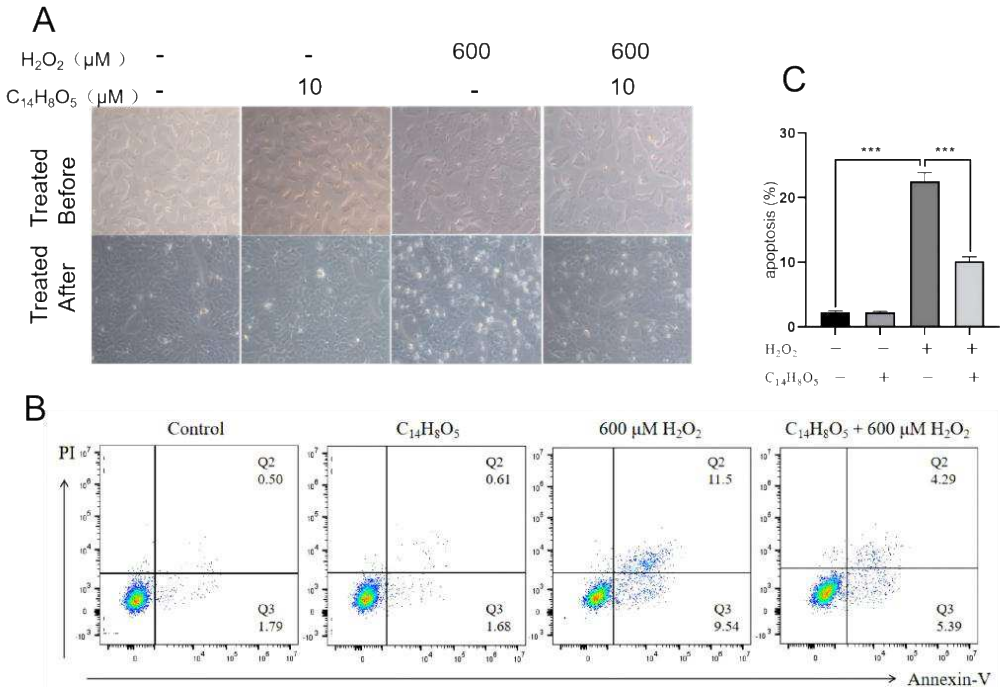

Figure 5. (A) Morphological changes of HaCaT cells before and after treatment the 10 μM C14H8O5，600 μM H_2O_2，10 μM C14H8O5 + 600 μM H_2O_2; the upper row represents cells before treatment, and the lower row represents cells treated with C14H8O5 and H_2O_2 for 24 hours. (B) HaCaT cell apoptosis results. (C)

Quantification of apoptosis. ***P<0.01 vs control group; ###P<0.01 vs 600 μM H_2O_2 treatment group

3.6 Hydroxylpurpurin Modulates Endocannabinoid System Levels in HaCaT Cells after H_2O_2-Induced Injury

As shown in Figure 5A-D, treatment with 600 μM H_2O_2 resulted in increased levels of the endocannabinoids OEA and PEA ($P < 0.05$), whereas the levels of AEA and 2-AG showed no significant changes. Compared with the H_2O_2 treatment group, pretreatment with 10 μM Hydroxylpurpurin led to a significant decrease in OEA levels ($P < 0.05$), no obvious changes in AEA and 2-AG levels, and a marked increase in PEA levels ($P < 0.05$). These findings suggest that the protective effect of hydroxylated alizarin against oxidative stress may be associated with increased PEA and decreased OEA levels in HaCaT cells. The endocannabinoid system (ECS) is an important component of skin immune regulation. Previous studies have reported that although PEA does not directly bind to CB1 or CB2 receptors, it can potentiate the effects of AEA and activate peroxisome proliferator-activated receptor-α (PPAR-α). In this study, the increase in PEA accompanied by a decrease in OEA preliminarily suggests that the protective mechanism of hydroxylated alizarin is closely related to the regulation of specific endocannabinoid ligand levels.

As shown in Figure 6E-F, the gene expression levels of the ECS receptors CB1 and CB2 are presented for each group. Compared with the control group, CB1 and CB2 expression levels were significantly increased in the 600 μM H_2O_2 treatment group ($P < 0.05$). In contrast, pretreatment with 10 μM Hydroxylpurpurin significantly reduced CB1 expression ($P < 0.05$) while further increasing CB2 expression ($P < 0.01$). These results suggest that the antioxidative stress effect of hydroxylated alizarin may be associated with suppression of CB1 expression and enhancement of CB2 expression. Previous studies have shown that increased CB1 expression can exacerbate oxidative stress and inflammation, and that AEA acting through CB1 often induces apoptosis. The present findings indicate that hydroxylated alizarin antagonizes oxidative stress–induced injury at the receptor level by inhibiting CB1 while promoting CB2 expression.

As shown in Figure 6G-J, the gene expression levels of the ECS ligand synthesis enzyme N-acyl phosphatidylethanolamine-specific phospholipase D (NAPE-PLD, NPLD) and the degradation enzymes FAAH, NAAA, and ASAH were analyzed. Compared with the control group, the expression of the degradation enzyme ASAH was significantly decreased in the 600 μM H_2O_2 treatment group ($P < 0.01$), while the expression levels of the synthesis enzyme NPLD and the degradation enzyme FAAH were markedly increased ($P < 0.0001$); no significant differences were observed in NAAA expression among the groups. Compared with the H_2O_2 treatment group, pretreatment with 10 μM Hydroxylpurpurin significantly reduced NPLD expression ($P < 0.05$) and markedly increased the expression levels of FAAH and ASAH ($P < 0.05$), whereas NAAA expression remained unchanged. These results indicate that the antioxidative stress effect of hydroxylated alizarin may involve suppression of the ECS ligand synthesis enzyme NPLD and enhancement of the degradation enzymes FAAH and ASAH. Changes at the enzymatic level represent the fundamental basis for alterations in ligand levels. Hydroxylated alizarin may re-establish ECS homeostasis under oxidative stress conditions by coordinately regulating the gene expression of synthesis enzymes (inhibiting NPLD) and degradation enzymes (enhancing FAAH and ASAH).

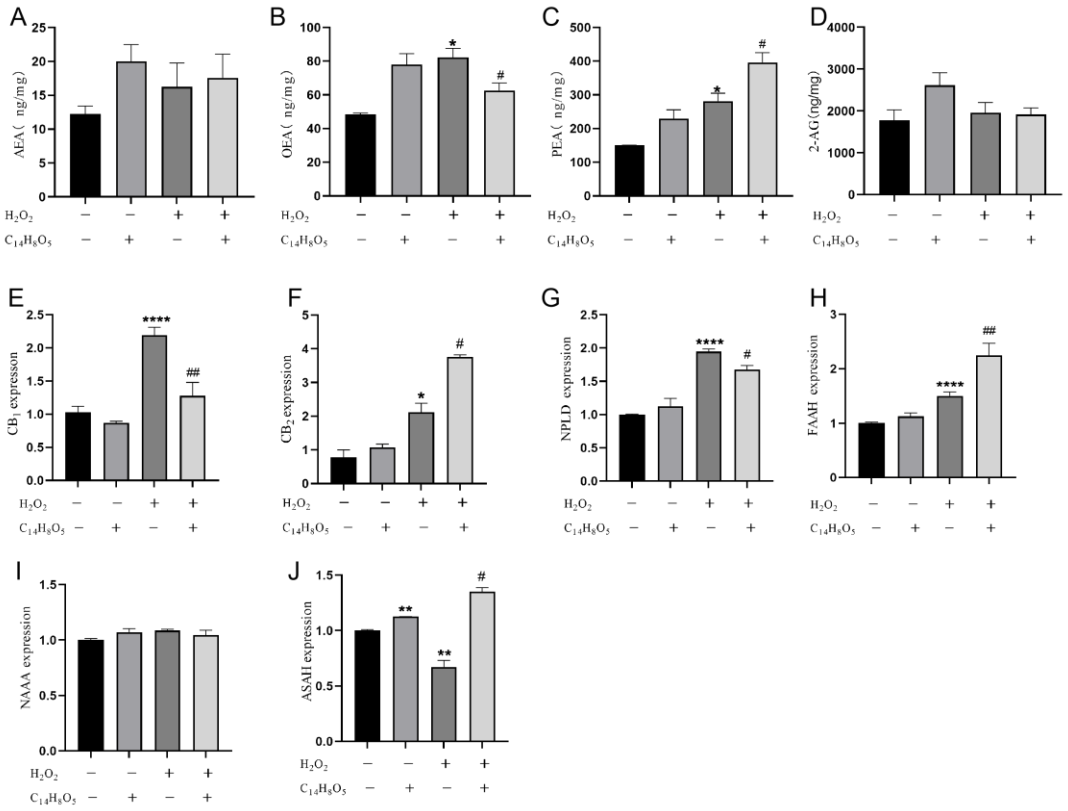

Figure 6. (A-D) Changes in the content of endogenous cannabinoids in HaCaT cells. (E-F) Expression of ECS receptor genes. (G-J) Expression of ECS related enzyme genes group. *P<0.05, **P<0.01 ,****P < 0.0001 vs control group; #P<0.05, ##P<0.01vs 600 μM H_2O_2 treatment group.

Conclusion

This study systematically investigated the protective effects and molecular mechanisms of Hydroxylpurpurin against oxidative stress–induced skin injury through an integrated strategy combining network pharmacology prediction, molecular docking simulation, and in vitro cellular experiments. Network pharmacology analysis and PPI network screening identified 75 key overlapping targets and revealed the PI3K/AKT signaling pathway as the central pathway mediating the pharmacological effects of hydroxylated alizarin. Subsequent molecular docking analyses further confirmed, at the molecular level, that hydroxylated alizarin exhibits strong binding affinity toward PIK3CA and AKT1, forming stable complexes through hydrophobic interactions and hydrogen bonding.

In terms of biological validation, a HaCaT cell oxidative injury model induced by 600 μM H_2O_2 was successfully established. Experimental results demonstrated that pretreatment with 10 μM hydroxylated alizarin markedly reduced intracellular ROS accumulation, improved cellular morphology, and significantly decreased the apoptosis rate (from 21.08% to 9.58%), indicating a pronounced cytoprotective effect. Further mechanistic investigations revealed that the antioxidative stress activity of hydroxylated alizarin is closely associated with extensive modulation of the endocannabinoid system (ECS). Specifically, hydroxylated alizarin suppressed the gene expression of the synthesis enzyme NPLD while enhancing the expression of the degradation enzymes FAAH and ASAH, thereby precisely regulating the metabolic balance of endocannabinoid ligands such as PEA and OEA. In parallel, hydroxylated alizarin effectively reversed oxidative stress–induced receptor imbalance by significantly downregulating the CB1 receptor, which is associated with oxidative damage and apoptosis, and upregulating the cytoprotective CB2 receptor.

In summary, hydroxylated alizarin effectively counteracts oxidative stress–induced injury in HaCaT cells by stably interacting with key targets in the PI3K/AKT signaling pathway and coordinately regulating the homeostasis of endocannabinoid ligands, receptors, and metabolic enzymes. These findings not only elucidate the multidimensional molecular mechanisms underlying the protective effects of hydroxylated alizarin on skin cells but also provide solid scientific evidence supporting its potential development as a novel antioxidant, anti–skin injury therapeutic agent, or functional cosmetic ingredient.

Fundings

This work was supported by Fujian Provincial Natural Science Foundation (Grant No. 2024J011399), Xiamen Municipal Medical and Health Guidance Program(Grant No. 3502Z20244ZD2020，3502Z20244ZD1155，3502Z20244ZD1259) and University Innovation and Entrepreneurship Project (Grant No.202512631074，202412631071).

Declaration of interests

None of the authors have any potential financial conflicts of interest related to this manuscript.

Reference

1. Zhou, R.; Wang, X.; Li, N., Overexpression of PBX1 attenuates oxidative stress and apoptosis in diabetic cardiomyopathy by transcriptionally inhibiting TXNIP. *Int J Biochem Cell Biol* **2025,** *186*, 106828.
2. Schieber, M.; Chandel, N. S., ROS function in redox signaling and oxidative stress. *Curr Biol* **2014,** *24* (10), R453-62.
3. Liu, H. M.; Cheng, M. Y.; Xun, M. H.; Zhao, Z. W.; Zhang, Y.; Tang, W.; Cheng, J.; Ni, J.; Wang, W., Possible Mechanisms of Oxidative Stress-Induced Skin Cellular Senescence, Inflammation, and Cancer and the Therapeutic Potential of Plant Polyphenols. *Int. J. Mol. Sci.* **2023,** *24* (4).
4. Śledziński, P.; Nowak-Terpiłowska, A.; Zeyland, J., Cannabinoids in Medicine: Cancer, Immunity, and Microbial Diseases. *Int. J. Mol. Sci.* **2020,** *22* (1).
5. Tsang, P. W.; Wong, A. P.; Yang, H. P.; Li, N. F., Hydroxylpurpurin triggers caspase-independent apoptosis in Candida dubliniensis biofilms. *PLoS One* **2013,** *8* (12), e86032.
6. Howlett, A. C.; Barth, F.; Bonner, T. I.; Cabral, G.; Casellas, P.; Devane, W. A.; Felder, C. C.; Herkenham, M.; Mackie, K.; Martin, B. R.; Mechoulam, R.; Pertwee, R. G., International Union of Pharmacology. XXVII. Classification of cannabinoid receptors. *Pharmacol. Rev.* **2002,** *54* (2), 161-202.
7. Carracedo, A.; Geelen, M. J.; Diez, M.; Hanada, K.; Guzmán, M.; Velasco, G., Ceramide sensitizes astrocytes to oxidative stress: protective role of cannabinoids. *Biochem J* **2004,** *380* (Pt 2), 435-40.
8. Gallelli, C. A.; Calcagnini, S.; Romano, A.; Koczwara, J. B.; de Ceglia, M.; Dante, D.; Villani, R.; Giudetti, A. M.; Cassano, T.; Gaetani, S., Modulation of the Oxidative Stress and Lipid Peroxidation by Endocannabinoids and Their Lipid Analogues. *Antioxidants (Basel, Switzerland)* **2018,** *7* (7).
9. Matkowski, A.; Jamiołkowska-Kozlowska, W.; Nawrot, I., Chinese medicinal herbs as source of antioxidant compounds--where tradition meets the future. *Curr. Med. Chem.* **2013,** *20* (8), 984-1004.
10. Shen, X.; Liu, A.; Li, L.; Zhu, J.; Yuan, J.; Wu, L.; Zhang, X., Robinin decreases myocardial ischemia/reperfusion injury via Nrf2 anti-oxidative effects mediated by Akt/GSK3β/Fyn in hypercholesterolemic rats. *J. Mol. Histol.* **2025,** *56* (5), 301.
11. Sun, H.; Wei, Y.; Deng, H.; Xiong, Q.; Li, M.; Lahiri, J.; Fang, Y., Label-free cell phenotypic profiling decodes the composition and signaling of an endogenous ATP-sensitive potassium channel. *Sci. Rep.* **2014,** *4*, 4934.
12. Luo, H.; Qin, W.; Zhang, H.; Ren, F. C.; Fang, W. T.; Kong, Q. H.; Yang, L.; Zhang, J. M.; Fang, C. W.; Hu, J. M.; Liu, S. J., Anthraquinones from the Aerial Parts of Rubia cordifolia with Their NO Inhibitory and Antibacterial Activities. *Molecules* **2022,** *27* (5).
13. Wen, M.; Chen, Q.; Chen, W.; Yang, J.; Zhou, X.; Zhang, C.; Wu, A.; Lai, J.; Chen, J.; Mei, Q.; Yang, S.; Lan, C.; Wu, J.; Huang, F.; Wang, L., A comprehensive review of Rubia cordifolia L.: Traditional uses, phytochemistry, pharmacological activities, and clinical applications. *Front. Pharmacol.* **2022,** *13*, 965390.

14. Bana, S.; Kumar, N.; Sartaj, A.; Alhalmi, A.; Qurtam, A. A.; Nasr, F. A.; Al-Zharani, M.; Singh, N.; Gaur, P.; Mishra, R.; Bhardwaj, S.; Ali, H.; Goel, R., Rubia cordifolia L. Attenuates Diabetic Neuropathy by Inhibiting Apoptosis and Oxidative Stress in Rats. *Pharmaceuticals (Basel)* **2023,** *16* (11).

15. Xia, M.; Li, Z.; Yang, C.; Wang, Y.; Zhang, J.; Zhong, G.; Ouyang, H.; Feng, Y., Rubia cordifolia L. extract ameliorates vitiligo by inhibiting the CXCL10/CXCL9/STAT1 signaling pathway. *J. Ethnopharmacol.* **2025,** *350*, 120027.

16. Ma, L.; Hu, P.; Zhang, J.; Cui, W.; Zhao, X., Hydroxylpurpurin exerted antidepressant-like effects on behavior and stress axis reactivity: evidence of serotonergic engagement. *Psychopharmacology (Berl.)* **2020,** *237* (3), 887-899.

17. Lajkó, E.; Bányai, P.; Zámbó, Z.; Kursinszki, L.; Szőke, É.; Kőhidai, L., Targeted tumor therapy by Rubia tinctorum L.: analytical characterization of hydroxyanthraquinones and investigation of their selective cytotoxic, adhesion and migration modulator effects on melanoma cell lines (A2058 and HT168-M1). *Cancer Cell Int.* **2015,** *15*, 119.

18. Zhu, Z. G.; Jin, H.; Yu, P. J.; Tian, Y. X.; Zhang, J. J.; Wu, S. G., Mollugin inhibits the inflammatory response in lipopolysaccharide-stimulated RAW264.7 macrophages by blocking the Janus kinase-signal transducers and activators of transcription signaling pathway. *Biol. Pharm. Bull.* **2013,** *36* (3), 399-406.

19. Li, Q.; Gao, J.; Pang, X.; Chen, A.; Wang, Y., Molecular Mechanisms of Action of Emodin: As an Anti-Cardiovascular Disease Drug. *Front. Pharmacol.* **2020,** *11*, 559607.

20. Jamaludin, R.; Kim, D. S.; Salleh, L. M.; Lim, S. B., Kinetic Study of Subcritical Water Extraction of Scopoletin, Alizarin, and Rutin from Morinda citrifolia. *Foods (Basel, Switzerland)* **2021,** *10* (10).

21. Gfeller, D.; Grosdidier, A.; Wirth, M.; Daina, A.; Michielin, O.; Zoete, V., SwissTargetPrediction: a web server for target prediction of bioactive small molecules. *Nucleic Acids Res* **2014,** *42* (Web Server issue), W32-8.

22. Safran, M.; Dalah, I.; Alexander, J.; Rosen, N.; Iny Stein, T.; Shmoish, M.; Nativ, N.; Bahir, I.; Doniger, T.; Krug, H., GeneCards Version 3: the human gene integrator. *Database* **2010,** *2010*, baq020.

23. Hamosh, A.; Scott, A. F.; Amberger, J. S.; Bocchini, C. A.; McKusick, V. A., Online Mendelian Inheritance in Man (OMIM), a knowledgebase of human genes and genetic disorders. *Nucleic Acids Res.* **2005,** *33* (suppl_1), D514-D517.

24. Wishart, D. S.; Knox, C.; Guo, A. C.; Shrivastava, S.; Hassanali, M.; Stothard, P.; Chang, Z.; Woolsey, J., DrugBank: a comprehensive resource for in silico drug discovery and exploration. *Nucleic Acids Res* **2006,** *34* (Database issue), D668-72.

25. Szklarczyk, D.; Gable, A. L.; Lyon, D.; Junge, A.; Wyder, S.; Huerta-Cepas, J.; Simonovic, M.; Doncheva, N. T.; Morris, J. H.; Bork, P., STRING v11: protein–protein association networks with increased coverage, supporting functional discovery in genome-wide experimental datasets. *Nucleic Acids Res.* **2019,** *47* (D1), D607-D613.

26. Addie, M.; Ballard, P.; Buttar, D.; Crafter, C.; Currie, G.; Davies, B. R.; Debreczeni, J.; Dry, H.; Dudley, P.; Greenwood, R.; Johnson, P. D.; Kettle, J. G.; Lane, C.; Lamont, G.; Leach, A.; Luke, R. W.; Morris, J.; Ogilvie, D.; Page, K.; Pass, M.; Pearson, S.; Ruston, L., Discovery of 4-amino-N-[(1S)-1-(4-chlorophenyl)-3-hydroxypropyl]-1-(7H-pyrrolo[2,3-d]pyrimidin-4-yl)piperidine-4-carboxamide (AZD5363), an orally bioavailable, potent inhibitor of Akt kinases. *J. Med. Chem.* **2013,** *56* (5), 2059-73.

27. Methot, J. L.; Achab, A.; Christopher, M.; Zhou, H.; McGowan, M. A.; Trotter, B. W.; Fradera, X.; Lesburg, C. A.; Goldenblatt, P.; Hill, A.; Chen, D.; Otte, K. M.; Augustin, M.; Shah, S.; Katz, J. D., Optimization of Versatile Oxindoles as Selective PI3Kδ Inhibitors. *ACS Med. Chem. Lett.* **2020,** *11* (12), 2461-2469.

28. Halgren, T. A., Merck molecular force field. I. Basis, form, scope, parameterization, and performance of MMFF94. *J. Comput. Chem.* **1996,** *17* (5‐6), 490-519.

29. Eberhardt, J.; Santos-Martins, D.; Tillack, A. F.; Forli, S., AutoDock Vina 1.2. 0: New docking methods, expanded force field, and python bindings. *J. Chem. Inf. Model.* **2021,** *61* (8), 3891-3898.

30. DeLano, W. L., Pymol: An open-source molecular graphics tool. *CCP4 Newsletter on protein crystallography* **2002,** *40* (1), 82-92.

31. Ravindranath, P. A.; Forli, S.; Goodsell, D. S.; Olson, A. J.; Sanner, M. F., AutoDockFR: Advances in Protein-Ligand Docking with Explicitly Specified Binding Site Flexibility. *PLoS Comput. Biol.* **2015,** *11* (12), e1004586.